Journal of The
Electrochemical Society

Novel Methodology of General Scaling-Approach Normalization of Impedance Parameters of Insertion Battery Electrodes – Case Study on Ni-Rich NMC Cathode: Part II. Detailed Analysis Using a Transmission Line Model

To cite this article: Marko Firm *et al* 2024 *J. Electrochem. Soc.* **171** 120543

Journal of The Electrochemical Society, 2024 **171** 120543

Novel Methodology of General Scaling-Approach Normalization of Impedance Parameters of Insertion Battery Electrodes – Case Study on Ni-Rich NMC Cathode: Part II. Detailed Analysis Using a Transmission Line Model

Marko Firm,[1,2] Jože Moškon,[1,z] Robert Dominko,[1,2] and Miran Gaberščček[1,2,z]

[1]*Department of Materials Chemistry, National Institute of Chemistry, 1000 Ljubljana, Slovenia*
[2]*Faculty of Chemistry and Chemical Technology University of Ljubljana, 1000 Ljubljana, Slovenia*

Here, we extend the general approach shown in PART-1 to a detailed analysis of the measured data using our previously published physics-based transmission line model (TLM). We construct general relationships between the TLM parameters and the electrode mass. We then systematically check the scaling properties of all model parameters by fitting the measured impedance responses of 8 NMC-NMC cells with different masses (thicknesses) of NMC cathodes ranging from 2.3 to 58.5 mg per 2 cm^2 of geometric electrode surface. We consider in detail all deviations of the measured spectra from the idealized spectra predicted by the model. Among other things, we discuss the high-frequency inductive effects, the ambiguities in the analysis of the low-frequency diffusion phenomena, and the effects of non-ideal capacitive properties (the so-called constant-phase elements) on the shape of the measured spectra. We also report an unexpected additional feature observed in measurements on thin (light) electrodes: a diffusion arc due to the diffusion of lithium in the electrolyte in the micropores of the NMC aggregates in the material used. Finally, we present a detailed dependence of all model parameters on the mass (thickness) of the electrode and discuss the potential practical significance of such an analysis.

 [DOI: 10.1149/1945-7111/ada060]

Manuscript submitted August 21, 2024; revised manuscript received October 31, 2024. Published December 30, 2024.

Supplementary material for this article is available online

In PART-1 of this paper, we introduced a broadly applicable experimental methodology and analysis strategy to assist battery researchers in conducting precise measurements and ensuring self-consistent parameter verification when analyzing the impedance data of lithium-ion insertion electrodes. As a model system, we selected a Ni-rich NMC insertion electrode to demonstrate the approach.

In this part (PART-2) we extend the general methodology presented in PART-1. First, we present a general transmission line model (TLM) developed in our earlier work[1,2] for analyzing impedance spectra of porous insertion electrodes. This model is then used to construct quantitative relationships between selected TLM parameters and electrode mass. We then use these relationships for a quantitative analysis of the impedance spectra of various NMC electrodes. Specifically, we analyze the impedance responses of eight symmetric NMC-NMC cells with different masses (thicknesses) of NMC cathodes, ranging from 2.3 mg to 58.5 mg per 2 cm^2 of geometric electrode surface area. In order to make the analysis as deterministic as possible, we fix only 13 values of the model parameters, while the other 91 values obtained from 8 samples are calculated based on the respective scaling laws explained in the first part of this paper. Good agreement in shape and magnitude is obtained between the measured and simulated impedance responses. The practical significance of the observed scaling trends of all model parameters is also discussed.

Experimental

Materials and methods.—We mainly use some of the measurements already discussed in PART-1. In the continuation, we repeat the essential information necessary for a better understanding of selected Ni-rich NMC active material, cells and procedures used to obtain the present impedance spectra.

NMC active material.—The Lithium Nickel Manganese Cobalt Oxide (NMC) material was provided by MSE Supplies® and was used in the form in which it was supplied (no treatment). Elemental analysis (ICP-OES) revealed the composition $LiNi_{0.83}Mn_{0.06}Co_{0.11}O_2$ (oxygen content assumed). The particle size distribution of the NMC material was analyzed on the SEM image at 400x magnification. For segmentation, QuPath software was used to manually delineate 500 particles within the visible area. Binary masks (black and white) were then exported from QuPath for each marked particle. A custom Python script was used to determine the areas and perimeters of the particles and derive their circularities and the diameters of the equivalent spheres (see PART-1).

Electrode preparation.—NMC powder, carbon black (Super C65T, Imerys), and PolyVinylene DiFluoride (PVDF, Sigma Aldrich) in mass ratio 90:5:5 were mixed together with N-Methyl-2-Pyrrolidone (NMP, Merck) in a shaker mixer/mill (SPEX SamplePrep) for 60 min. The resulting ink (slurry) was applied to carbon-coated aluminum foil (Armor, France) using a doctor blade mounted on an automatic coating machine (MTI Corporation). The coated electrode film was first dried at 80 °C in a dynamic vacuum for at least 3 h. The final NMC coating had a mass loading ranging from 0.7 to 31 $mg{\cdot}cm^{-2}$. The circular cathodes with a geometric area of 2 cm^2 were cut and pressed with a hydraulic hand press (Specac) with a force of 1.25 $t{\cdot}cm^{-2}$ (resulting in a typical porosity of about 40%). The final thickness of the cathodes ranged from 15 μm for the thinnest to 140 μm for the thickest electrodes. In a second step, the cathodes were dried overnight under dynamic vacuum at 110 °C and transferred to an argon-filled glove box (MBraun) with a water and oxygen content of less than 1 ppm. The anodes were prepared in a glove box from a 200 μm thick lithium metal foil (Gelon), which was cut into circles with an area of 2.5 cm^2. The lithium surface was carefully scraped and rolled to expose a fresh metal surface. To perform the so-called 3-electrode impedance measurements, a 4 cm long and 50 μm thick Au wire with a 7 μm thick insulating layer of polyimide (Goodfellow) was used. On one side, 0.3 mm of the insulation was removed by heat treatment. On the other side, the wire was spot-welded to a copper (20 μm foil) current collector.

Electrode porosity.—The porosity of the cathodes was calculated based on the mass, thickness, composition and physical densities of

[z]E-mail: joze.moskon@ki.si; miran.gaberscek@ki.si

the composite components. The thickness was determined using a gauge (Garant). To validate the accuracy of the porosity calculations, Mercury intrusion porosimetry (MIP) was performed on samples with different mass loadings (5 mg·cm^{-2}, 11 mg·cm^{-2}, and 22 mg·cm^{-2}). The measurements were carried out with the AutoPore IV 9500 porosimeter (Micromeritics). The sample weight was typically 0.36 g. The porosimeter operated in a pressure range of 0.004–413 MPa, corresponding to a pore size of 403 μm to 0.0037 μm, based on the Washburn model. The measurements were carried out in two stages: first in the low-pressure regime (0.004–0.345 MPa) and then in the high-pressure regime (0.1–413 MPa). Since the D90 value (SEM) is (21.8 ± 0.7) μm, only diameters of less than 22 μm were considered as cathode porosity. The pore/void volume filled at lower pressures (larger diameter) corresponds to the penetration of Mercury into the space between the electrodes in a measured sample.[3]

Cell assembly.—The pouch cells were assembled in glove box filled with Ar by properly stacking the electrodes and separator and sealing them in a Triplex foil with pre-prepared 3 mm wide foil strips for the contacts (Al for the cathode, Cu for the anode and RE in 3-electrode cells). The separator used was glass microfiber filter paper GF/A (Whatman) with a thickness of 260 μm (manufacturer specification) which was compressed to the final thickness of about 208 μm during assembly into the pouch cell (the calculated porosity was 88%). The geometric surface area of the separator was 3.14 cm^2. Commercially prepared 1 M $LiPF_6$ in EC/DEC = 1:1 vol (LP40, E-lyte) solution was used as electrolyte. In 3-electrode cells with gold microwire RE, 1 M $LiPF_6$ in EC/EMC = 3:7 vol (LP57, E-lyte) solution was used. The electrolyte was distributed as follows: 1 μl per mg of active material for the cathode (or minimum 10 μl), 15 μl for the Li anode and 70 μl for the separator. In the 3-electrode NMC‖RE(Au)‖CE(Li) cell, 270 μl of electrolyte was added for 2 separators. Symmetric NMC-NMC and Li-Li cells were assembled from two starting (pre-cycled) Li-NMC cells with matching NMC mass loading. For the preparation of the NMC-NMC cells, a fresh separator and a fresh electrolyte were used in a similar manner as for the NMC-Li cells (1 μl per mg of active material (or minimum 10 μl), and 70 μl for the separator), followed by sealing in a pouch-bag cell.

Electrochemical measurements.—The NMC-Li cells were first pre-cycled to complete the initial "formation" processes (e.g. the observed initial "activation" of the NMC material). The cells were cycled for 3 cycles in CC-CV charge and CC-discharge mode between 2.8 V and 4.3 V (vs Li). The first cycle was performed at a current density of C/15, followed by 2 cycles of C/10 and a 3 h open circuit relaxation. After relaxation, the cells were discharged to 2.8 V with C/20 to achieve a reproducible lithiated state, and finally a C/20 charge step up to 3.805 V was performed, followed by a 6 h voltage hold. Subsequently, the NMC Li cells were placed in a glove box filled with Ar, disassembled, and the cathodes were used to fabricate the corresponding NMC Ni cells (as described above). A potential controlled impedance measurement (PEIS) was performed with a perturbation with an amplitude of 5 mV (3.5 mV rms) in the frequency range from 1 MHz down to 0.1 mHz. Galvanostatic curves and impedance spectra of the cell were measured at room temperature (24 °C) using a VMP3 potentiostat/galvanostat (BioLogic) with built-in impedance module.

Theoretical

General transmission line model (TLM) for porous insertion battery electrodes.—Impedance response of present symmetric NMC-NMC cells containing porous NMC electrodes separated with electrolyte-soaked glass fiber separator is analysed by assuming the generalized cell structure shown in Fig. 1a and using our previously published physics based transmission line model (TLM).[1,2] The simplified planar version (Fig. 1b) was used where

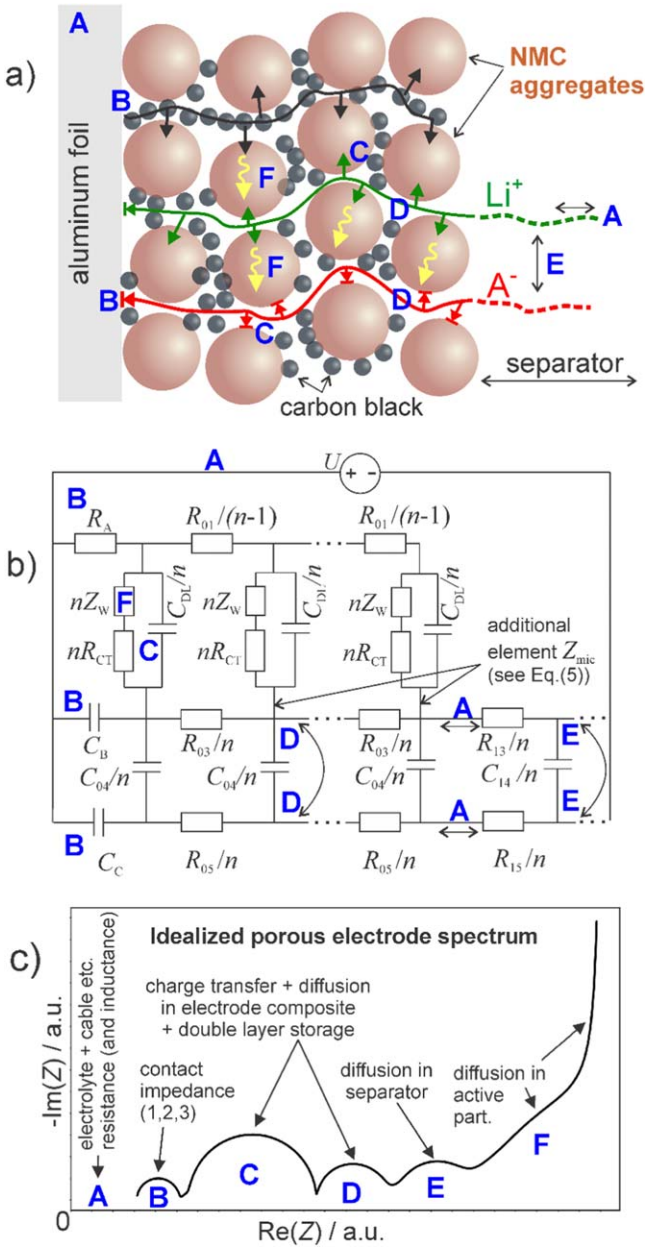

Figure 1. (a) Provisional general scheme of porous cathode and the main processes (indicated by arrows) that can be probed using EIS. (b) Basic model used for simulations shown in this work (according to refs. 1, 2). The meaning of elements is explained in the main text. (c) Theoretically expected impedance response of the porous electrode based on the model in panel (b). Letters A-F connect the main processes expected in the porous electrode with the model and the corresponding impedance response.

the elements describing ambipolar diffusion of lithium ions and electrons (lithium component) inside solid NMC particles (see Fig. 2b in[1]) were replaced with an appropriate Warburg element (Z_W in Fig. 1b). In fact, due to diffusion anomalies caused by variations in the size of the primary particles, mutual crystal lattice orientation of neighboring particles, variations in micropore content in NMC aggregates, unclear geometry of lithium diffusion within the particles (radial vs planar, etc.), we further replaced the Warburg element with a series of arbitrary elements that, however, numerically matched quite well to the measured diffusion impedance, as explained in the chapter that introduces the combined approach to analysis of measured EIS spectra. All the other elements were explained in detail in our previous publication.[1] Briefly, their

meaning is the following: R_A is the contact resistance between the current collector and cathode composite, R_{01} is the average electronic resistance of the cathode, C_B and C_C are the capacitive contributions of active and non-active ions, respectively, to the total capacitance of the double layer formed at the contact between electrolyte and current collector, R_{CT} is the charge transfer resistance due to incorporation of active species from the electrolyte into the solid active NMC particles, C_{DL} is the double layer capacitance due to interface between the electrolyte phase and electronic conductors (carbon black, NMC particles), R_{03} and R_{05} are the resistances for movement of lithium ion and counter anion in the porous electrode, C_{04} is the chemical capacitance of the electrolyte in porous electrode, R_{13} and R_{15} are the resistances for movement of active ion (lithium ion) and counter anion in the separator, and C_{14} is the chemical capacitance of electrolyte in separator.

The main idea of the present paper was presented in the PART-1 of this paper: By varying the mass loading (thickness) of the electrode composite and measuring the corresponding impedance spectra, one should be able to test the validity of existing porous electrode models for interpreting the realistic impedance response of a state of the art porous cathode such as NMC. Such a test namely directly involves the variation of almost all relevant model parameters: (i) the parameters related to the interface with the aluminum foil (R_A, C_B, C_C) and the bulk electrolyte parameters (R_{13}, C_{14} and R_{15}) are independent of the mass loading (thickness) of the cathode composite, (ii) the parameters describing the transport resistance across the whole composite (R_{01}, R_{03} and R_{05}) are assumed to scale proportionally to the thickness of the composite (and not exactly proportional to the mass loading, as will be shown later), (iii) parameters related to the properties of the interface between the ionic conductor (electrolyte) and the electronic conductor (mainly carbon black) within the porous electrode structure (R_{CT}, C_{DL} and Z_W) are inversely proportional to the electrode thickness and (iv) the chemical capacitance due to the electrolyte in the pores (C_{04}) is proportional to the electrolyte volume.[4]

The calculations of the impedance spectra from the TLM shown in Fig. 1b were carried out using the well-known mesh method which assigns the so-called mesh currents in the essential meshes of the circuit. Using the Kirchhoff 's voltage law a set of equations is obtained that link the mesh currents to the voltage source, U, through all the elements of TLM. The impedance of transmission line is then readily calculated as U / J_0 where J_0 is the current through the main loop of the scheme. Typically, 200 current loops were created for each sector (cathode1, separator, cathode2) (i.e. n = 200 in scheme in Fig. 1b). The relative error of resulting simulated impedance responses was about 0.5% (the error was determined by comparing the absolute value of simulated impedance at given frequency and the corresponding exact solution for cases where the latter existed). To facilitate the understanding of mathematics behind the present simulation, we provide a typical code in Supporting information that presented the basis of present simulations.

Methodology of general scaling-approach normalization of impedance parameters based on TLM for porous insertion cathodes.—The novel TLM-based methodology of the general normalization of electrode impedance parameters according to the scaling approach is shown schematically in Fig. 2. Essentially, the proposed scaling approach provides means to logically relate the values of the individual parameters associated with the corresponding processes in a cell to the geometry of the cell components. Let us consider a case where the tested insertion electrode (WE) is on the left side, and in contact with a separator that separates our electrode from the counter electrode (CE) or reference electrode (RE) on the right side (not shown). The CE serves as a lithium source (provides Li^+ ions and electrons) and can be either a Li metal anode, a lithium-containing graphite anode or another lithium-containing anode. For impedance measurements it may even be used together with another (partially charged) cathode (symmetric cell). When used, RE should be reversible to Li^+ ions, and (in an idealized scenario) should not affect the distribution of ionic current lines passing through the plane in which RE is positioned. The TLM of a porous insertion electrode together with an adjacent separator (Fig. 2c) can be considered to be composed of $2n$ equivalent layers obtained by an imaginary process of slicing both the electrode and the separator into n layers of equal thickness, where the interfacial layer adjacent to the current collector is different and is assumed to describe the properties of this interface.[1] To achieve the desired accuracy of the simulated impedance spectra, n should be at least 100 (simulation time approx. 15 s), for more precise modeling n should be increased to about 300 (simulation time = 80 s). For a more detailed analysis of the accuracy of the TLM in battery analysis, see our previous work.[5]

In general, all important processes that take place in the system under consideration (Fig. 2) can be described by *5 scaling relationships*. The first two relations, (R.1) and (R.2), define the parameters that are independent of the thickness of the WE, but dependent on its cross-sectional area (S_e). The relationships (R.3), (R.4) and (R.5), consider parameters that are dependent on both the thickness of the WE (L_e) and the cross-sectional area (S_e).

Relations (R.1a) and (R.2a) quantify parameters related to the processes at the interface between the current collector and the electrode composite, and relations (R.1b) and (R.2b) quantify the processes in the separator. At the surface of the current collector, an electron transport from the current collector into the adjacent material of the electrode composite takes place during discharge, the resistance of which is described by R_A, which we refer to as "contact resistance."[6,7] In the electrolyte-soaked electrode, an electrical double layer forms at the current collector/electrolyte interface, which can be divided (arbitrarily) into the respective capacitances for cation (Li^+, C_B) and anion (A^-, C_C) contributions.[1] The transport properties of a separator soaked with liquid electrolyte can be described with two parallel rails, which describe the paths of the cations (Li^+, red) and anions (A^-, blue). The Li^+ ions move from right to left, the anions A^- in the opposite direction. The cations and anions are coupled locally via chemical capacitors (C_{14}/n) over the entire thickness of the separator. The paths of the ions are their effective paths—this means that the corresponding (integral) resistances ($n \times R_{13}/n$ for Li^+ and $n \times R_{15}/n$ for A^-) are linearly proportional to the thickness of the separator (L_{sep}), inversely proportional to the cross-sectional area of the separator (S_{sep}), and dependent on the porosity of the separator (ε_{sep}) and its tortuosity (τ_{sep}). In cases where the cross-sectional area of WE (S_e) is large compared to the thickness of the separator, it can be assumed that the ionic current through the separator has a cross-sectional area equal to $S_e \times \varepsilon_{sep}$, and accordingly the ionic resistances R_{13} and R_{15} can be expressed by the relation (R.2b), Fig. 2c). The integral chemical capacitance C_{14} scales with the volume of electrolyte in the separator (R.1b).

The relationships (R.3)–(R.5) define the parameters that are dependent on the WE thickness (L_e). The ion paths from the separator continue in the insertion WE, run along the electrode pores and branch out over the entire electrode thickness until they finally reach the surface of the current collector (they end in the double-layer blocking conditions, C_B and C_C). The paths of the two ions in the electrode composite, are not only (locally) coupled to each other (by chemical capacitances C_{04}/n), but also simultaneously with the paths of the electrons.[a] The ions (Li^+, A^-) and electrons are coupled to each other at the electrode/electrolyte interface by double-layer capacitances (C_{DL}/n). For a homogeneous electrode composite, the corresponding (integral) values, C_{04} and C_{DL}, scale with the electrode thickness (L_e) according to the relationships (R.3a) and (R.3b). The electrical resistance due to the electron flow originating from the current collector on the left side and branching along the conductive solid phases (AM particles mixed with electronically conductive additive(s)) that finally reach the junction

[a]The exact circuit should allow for direct coupling between anion rail and electron rail in electrode. In the planar circuit (Fig. 2c) only cations are directly coupled to the electron paths. We have shown in our previous work[1] that the planar circuit (Fig. 2c) actually very accurately describes impedance response of insertion electrodes.

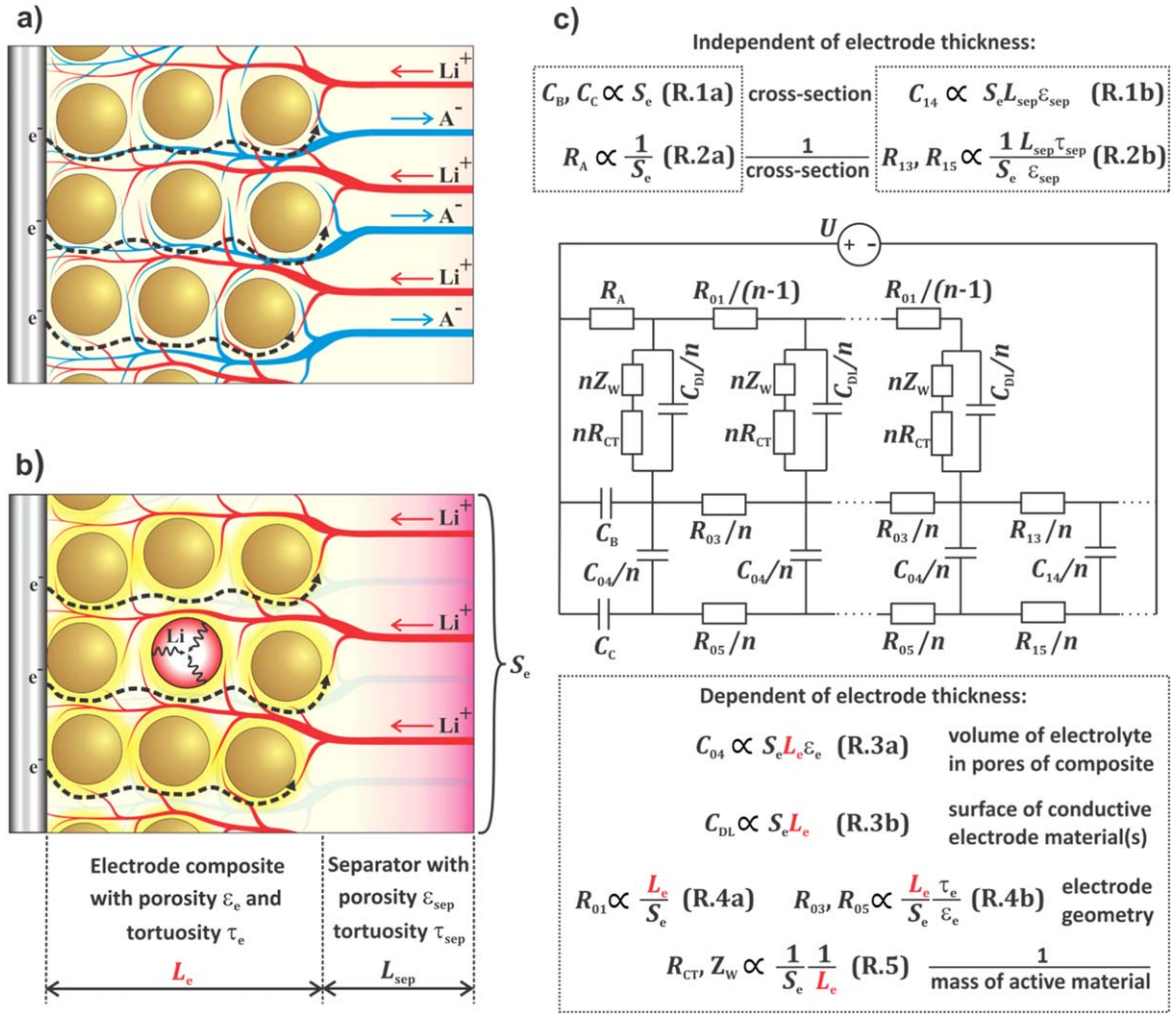

Figure 2. Schematic representation of the lithium-ion insertion cathode (WE) in contact with the electrolyte-soaked separator. The schematic highlights the ionic current lines in the liquid electrolyte phase at (a) short times (high frequencies) and (b) long times (low frequencies) when a near steady state is reached. (c) Expected (ideal) scaling relationships of the electrode and separator parameters in the corresponding equivalent TL model repeated from Fig. 1 to facilitate the identification of the position of a particular parameter in TLM. For the sake of simplicity, the carbon black as a conductive additive and the binder are not shown in the diagram. Although the binder is not explicitly included in the model, the effects of the binder are not excluded (the associated effects are included/priced in the values of the electrode parameters obtained).

between the electrode and separator has been referred to as the electronic part of the "wiring" of an electrode. Similarly, the total ionic resistance due to the branching of the two ionic paths (Li^+ and A^-) within the porous system of the electrode has been referred to as the ionic part of the "wiring" of the electrode.[7–9] The "electronic wiring" of the electrode composite is quantified with the resistances R_{01}/n, while the "ionic wiring" is described by the resistances R_{03}/n (for Li^+) and R_{05}/n (for A^-). The integral resistance parameters of the two "wirings" depend on the electrode geometry and scale linearly with L_e according to the relationships (R.4a) and (R.4b).

In the case of a discharge step, a gradual transfer of coupled Li^+ ions and electrons into the interior of the AM particles begins to take place after a sufficiently long time and a sufficient rearrangement of the charge distribution in the double layer at the electrolyte/AM interface. The coupled de-solvation of Li^+ ions and the simultaneous electron transfer to redox centers at the surface of the AM particles is quantified with the "charge-transfer" resistance parameter ($n{\cdot}R_{CT}$). In response, a concentration-driven diffusion flow of coupled Li^+ and electrons takes place within the solid state of the AM particles (Fig. 2b). The latter process of coupled diffusion of Li^+ ions and electrons can be described by a general expression for finite-length ambipolar diffusion with blocking boundary in the case of a small-signal AC excitation (in a linear regime):[7,10,11]

$$Z_w = R_w \frac{1}{\sqrt{i\omega\tau}} \coth\sqrt{i\omega\tau}. \quad [1]$$

Parameter τ is the characteristic diffusional relaxation time that can be expressed as:

$$\tau = R_w C_w = \frac{L^2}{D^\delta}, \quad [2]$$

where R_w and C_w are the general resistance and chemical capacitance due to diffusion processes, L is the diffusion length and is of the same order of magnitude as the average particle size, and D^δ is the chemical diffusion coefficient of the neutral component lithium (other notations are also in use, $D^\delta = \tilde{D}_{Li} = D_{chem}$). It should be emphasized that Eqs. 2 and 3 only apply for AM with a single-phase lithium storage mechanism (e.g. via a solid solution). The expression in Eq. 2 is referred to as finite length/space Warburg impedance with blocking/open-end/reflecting boundary; in the literature these terms are used interchangeably and different abbreviations are used, e.g. FSW = Finite Space Warburg. Importantly for the present work, both interfacial, R_{CT}, and the volume, $Z_{W,ins}$, parameters of AM scale inversely with L_e according to the relationship (R.5).

Since the anion is not involved in the main electrochemical process, a gradual build-up of concentration gradients occurs in the liquid electrolyte during the discharge. This is because the concentration of the Li salt decreases in the areas adjacent to the particles of the cathode AM and simultaneously increases on the opposite side (e.g. at the anode particles in CE or at the cathode particles of CE in the case of symmetric cell), as shown schematically in Fig. 2b. Accordingly, the net flux of anions in the electrolyte gradually decreases due to the opposite diffusion flux of the salt LiA and finally decreases towards zero in the limiting case of very long times (and accordingly at very low frequencies) when a near steady state has been established (Fig. 2b). The porous structure of the separator and the finely porous cathode limit the natural convection in the electrolyte phase contained therein. Therefore, in this regime, practically the entire ionic current through the electrolyte is carried by Li^+ ions. Moreover, in the case of an electronically well conducting electrode (good "electronic wiring" corresponding to a low value of R_{01}), the total resistance of the cathode can be defined in the zero-frequency limit of the impedance measurement and expressed by a simple relationship[1]:

$$R_{\text{total}}(x) = \lim_{f\to 0}\{\text{Re}(Z)\} = R_A + R_{13} + R_{CT}(x) + R_{03}/3 + R_w(x)/\xi. \quad [3]$$

The parameter ξ introduces the dimensionality of the diffusion-based insertion process within the particles of AM, where ξ is 3, 4, and 5 for planar (1D), cylindrical (2D), and spherical (3D) symmetry, respectively.[12] The practical significance of this last relationship is explained in more detail in the Results and Discusion section. From the perspective of the present work, the key contributions are $R_{03}/3$ and $R_w(x)/\xi$, which measure the magnitudes of the total diffusion resistance of Li^+ ions in the electrolyte phase (within the cathode porosity) and the total diffusion resistance of the neutral component lithium (coupled Li^+ and electrons) in the solid state within the particles of AM. Note that $R_{\text{total}}(x)$ depends on the degree of electrode lithiation, which results from the fact that both $R_{CT}(x)$ and $R_w(x)/\xi$ are a function of x.

In a similar way to $R_{\text{total}}(x)$, we can also define the *total electrode capacitance* of an insertion cathode in the zero-frequency limit of the impedance measurement based on the discussion in PART-1. There the general insertion capacitance was defined as C^{δ}_{ins} which leads to the following expression:

$$C_{\text{total}}(x) = \lim_{f\to 0}\left\{\frac{1}{i\omega \bullet Im(Z)}\right\} = \lim_{f\to 0}\{C^{\delta}_{ins}(x,\omega)\} = \theta \bullet C_d(x), \quad [4]$$

where ω is the angular frequency ($\omega = 2\pi f$), $C_d(x)$ stands for the differential capacity of the cathode and θ is a capacity utilization factor that ranges from 0 to 1 and indicates what fraction of $C_d(x)$ can actually be achieved during the impedance perturbation for a given x. In PART-1 we have shown that for the Ni-rich NMC the values of θ are very close to 1 (or possibly even exactly 1); the only exception being the state at 3.55 V, where definite determination of $C_{\text{total}}(x)$ was not possible.

***Assumption of* homogeneous and continuous *electrode composite and* mass-normalization *of impedance spectra.*—**The TL equivalent circuit shown in Figs. 1b (and 2c) is exactly correct under the assumption that the electrode composite is *homogeneous and continuous* in its phase composition, internal morphology and structure. In practice, this means that the mixture of AM, conductive additive and binder should be ideally mixed, with an ordered arrangement and distribution of the pores and conductive additive, and that the AM particles should also be monodisperse. In addition, the distribution of ionic and electronic "wires" within the electrode porosity and along the solid phases should be ideal—i.e. the electrolyte should completely fill the voids and pores and uniformly "wet" the entire surface of the active particles; at the same time, the surface of the AM particles should be uniformly accessible to electrons via the conductive additive. The latter condition need not be completely fulfilled if AM has a high electrical conductivity or is uniformly coated with a conductive film (e.g. a carbon coating); alternatively, it is sufficient if the electronic conductivity of AM is significantly higher compared to its ionic conductivity.[13,14] Although the listed ideal conditions are often not completely fulfilled in the real electrodes (as discussed in the Results and Discussion section), it is very useful to consider the idealized case and investigate deviations from the ideal conditions.

From the relationships in Fig. 2c, it is easy to deduce that the *mass normalization* of the impedance spectra which is frequently used by many researchers simultaneously regulates all scaling relationships that include the electrode thickness parameter (L_e). Furthermore, if S_e is defined and kept constant, the parameters in relationships (R.3a), (R.3b) and (R.4a), (R.4b) scale linearly with L_e. If we further assume that the electrode composite is *homogeneous and continuous,* relations (R.3) and (R.4) show that the corresponding parameters (C_{04}, C_{DL}, R_{01}, R_{03}, R_{05}) scale linearly with the mass of AM. On the other hand, the two parameters related to the insertion active material (R_{CT} and $Z_{W,ins}$) scale inversely proportional to L_e (relation (R.5)). The relationship (R.5) can be expressed more precisely as:

$$R_{CT},\, Z_{W,ins} \propto \frac{1}{m_{AM}}. \quad [R.5a]$$

The value of R_{CT} is also influenced by the electrode composition, porosity and homogeneity, as well as other factors that affect the accessibility of electrons and Li^+ ions to the surface of the AM particles. Furthermore, the R_{CT} depends on the state of the AM/electrolyte interface, e.g. the formation and stability of the cathode-electrolyte interphase (CEI), as well as the structural rearrangement of the AM surface. In contrast, the solid-state processes in the particles of the (non-degraded!) AM are expected to be only slightly influenced by the electrode parameters. In other words, for insertion cathodes with AM in the "fresh" state[b] the relationship (R.5b), in combination with Eq. 4 implies:

$$m_{AM} \bullet \lim_{f\to 0}\{i\omega \bullet Im(Z)\} \propto m_{AM}/C^{\delta}_{ins}(x). \quad [R.6]$$

This relationship confirms the validity of the simple preliminary analysis of the mass-normalized EIS spectra in PART-1, where the anticipated relationship (Eq. 2, PART-1) was constructed on the basis of empirical (experimental) observations and the intuitive assumption of (idealized) capacitive charge storage in the active material.

In PART-1, we experimentally determined the zero-frequency limiting conditions of the insertion diffusion storage according to relation (R.6) and obtained the corresponding values of the normalized insertion capacitance (in F per 1 g AM) directly from the corresponding mass-normalized Nyquist plots. Note that the relation (R.6) is valid even if the assumption of homogeneity and continuity of the electrode composite is not fulfilled.

Use of scaling relationships and deviations from an ideal electrode—the case of NMC cathodes.—The observations made for an ideal electrode are very important when you try to analyze experimental EIS data. This is because the idealized model clearly shows that the individual impedance parameters of the TLM are strongly coupled, which greatly reduces the degrees of freedom and can prevent the undesirable mode of overparameterization. We can use this principle of coupled parameters to perform a physically meaningful and reliable analysis of the impedance spectra. The results of the microscopic analysis of the NMC particles and the

[b]Here "fresh" state of AM is referred to as state of electrode AM with no degradation (structural or other) damage took place; whereby all of the Li sites in the host structure can reversibly participate in the electrochemical (de)-lithiation.

corresponding electrodes (see PART-1) clearly show that the analyzed cathodes are not ideal.

In short, the NMC material used is in the form of aggregates with a rather large dispersion of aggregate sizes, which leads to an uneven volume packing of NMC in the cathodes, causing an uneven distribution of ionic pathways (electric field). In addition, a pronounced distribution of charge storage site accessibility within the crystallites of the aggregates must be considered—for example, small aggregates are preferentially (de)-lithiated, while the largest ones are only partially utilized. Another variable is the degree of cracking in the aggregates—with the overall effect that the size of the aggregates is effectively reduced. Important deviations are expected for the lowest mass loading cathodes, where the composites are unevenly compacted during pressing and porosity is less well defined; in the corresponding NMC-NMC cells, the electrolyte/NMC ratio will be higher compared to well compacted thicker cathodes. The (local) tortuosity of the electrode is another property that strongly influences the ion transport and consequently the spatial homogeneity of the utilization of an insertion electrode. All of the above effects can lead to one or more deviations from the expected scaling relationships for a hypothetical ideal electrode. Some of these effects are large, while others only affect the accuracy of the obtained impedance parameters, as explained below.

To summarize this part, we have presented a new general scaling relation between the elements of the transmission line model and the electrode mass (loading). While the relationships presented apply to homogeneous, uniform electrodes, we have also discussed some deviations that may occur with realistic porous insertion cathodes such as NMC.

Results and Discussion

The scaling properties of NMC electrodes were verified by analyzing a series of such electrodes with different masses ranging from about 2.3 mg to 58.5 mg (Table I) using the transmission line model presented in Fig. 1b. The geometric surface area of all electrodes was 2 cm^2. The measurements were performed on so-called symmetric cells, i.e. cells containing two NMC electrodes as similar as possible, separated by a glass fiber separator, and pores of both electrodes and separator were filled with 1 M $LiPF_6$ in EC/DEC = 1:1 vol. (LP40) electrolyte, as described in Experimental. The results for a single electrode were obtained by simply dividing the measured impedance values by 2.

As can be seen from Table I, the average thickness of the electrodes increases with the mass of the electrodes, although not exactly linearly. This is due to various factors that influence the manual (laboratory-scale) preparation of the electrodes and limitations presented by the finite size of NMC aggregates: particle size distribution analysis showed that D_{50}= (12.9±0.1) μm and D_{90}= (21.8 ± 0.7) μm (see PART-1). Similarly, the estimated volume of electrolyte in the electrode pores is expected to vary approximately linearly with mass loading, but some significant deviations from this expected trend occur, especially at smaller loads.

Table I. Set of the studied NMC-NMC symmetric cells with the cathode specifications. Volume of electrolyte contained within each cathode was calculated based on gravimetric porosity (ε_ρ) and cathode dimensions. *For the two cells with the thinnest cathodes the gravimetric porosity (ε_ρ) strongly deviates (is larger) due to non-effective pressing of the composites because in those two cases the cathode thickness was of comparable magnitude as the diameter of largest (non-cracked) aggregates (see explanation in main text).

No.	NMC mass [mg]	Cathode thickness [μm]	Cathode porosity ε_ρ [%]	Electrolyte volume [μl]
1	2.3	15	79*	3.6
2	5.0	20	67*	3.9
3	11.1	27	45	3.8
4	22.5	55	45	7.7
5	29.9	70	42	9.4
6	39.6	90	41	11.5
7	49.3	110	40	13.7
8	58.5	140	44	19.3

For the two thinnest cathodes, the gravimetric porosity (ε_ρ) is much higher (Table I) due to the ineffective pressing of the composites. This is due to the fact that when pressing the thinnest NMC cathodes, the largest spherical NMC aggregates are partially cracked and (morphologically) decomposed and at the same time effective compaction of the electrode composite is not possible. Moreover, the values of the measured cathode thicknesses (used for the calculation of ε_ρ) for these thinnest cathodes are strongly influenced by the prevailing largest (albeit cracked/disintegrated) NMC aggregates, which define the thickest spots/areas of the cathodes. Consequently, the corresponding calculated values of porosity are highly overestimated which is why these values are marked with an asterisk (*) in Table I. In the analysis of the present results, we have considered the actual scaling factors from Table I instead of assuming the idealized scaling relationships shown in Fig. 2.

Problems occurring in fitting the present spectra.—When comparing experimental trends with theoretical predictions, the most direct approach is to fit the measured spectra to the given model. In this particular study, the result of the fit would be a set of fitted model parameters and one could then determine whether the measured parameters follow the theoretical scaling relationships predicted in Fig. 2c. However, it turns out that fitting the measured spectra in the present case is not always straightforward and may even lead to significant inconsistencies. In the next sections, we explain the main problems encountered in fitting the present spectra and then propose an improved methodology for evaluating the measured data.

Let us first consider a spectrum theoretically predicted by the TLM, shown in Fig. 1c. To facilitate the discussion, we deliberately separated the different features (arcs, lines, etc.) and assign a rough physical meaning to each of the features (Fig. 1c). We see 6 different features, each of which is completely determined by one or two resistive parameters and a capacitance from the model. A brief analysis shows that by fitting such an ideal spectrum to the model, 12 (out of 13) of the model parameters included in Fig. 1b can be uniquely determined. In other words: If the value of only one model parameter is known independently, all other model parameters can be determined by fitting a single spectrum. This fact shows the great (theoretically expected) selectivity of impedance spectroscopy when used to analyze different processes in typical porous battery electrodes.

However, if we look at an average impedance measurement of NMC electrodes (Fig. 3), we see many deviations from the ideal model predictions. At the highest frequencies (around 1 MHz), an additional line can be seen extending downwards to positive values of the imaginary part of the impedance. This is usually attributed to inductive effects due to measuring device cables or metallic parts of the cell components. In addition, at the highest frequencies, a considerable scattering of the measurement points can occur (not seen in Fig. 3, but recognizable in some of the measurement curves shown in Figs. 6 and 7). Features B and C appear to roughly match the predicted theoretical spectrum in Fig. 1c, although some deviations of the measured spectra from the expected shape of arc C were observed (see the more detailed analysis in continuation). In contrast, features D, E and F appear to be strongly coupled, such that only a single hump (instead of two arcs and a 45-degree feature) is observed before the spectrum transitions to a vertical capacitive line at the lowest frequencies.

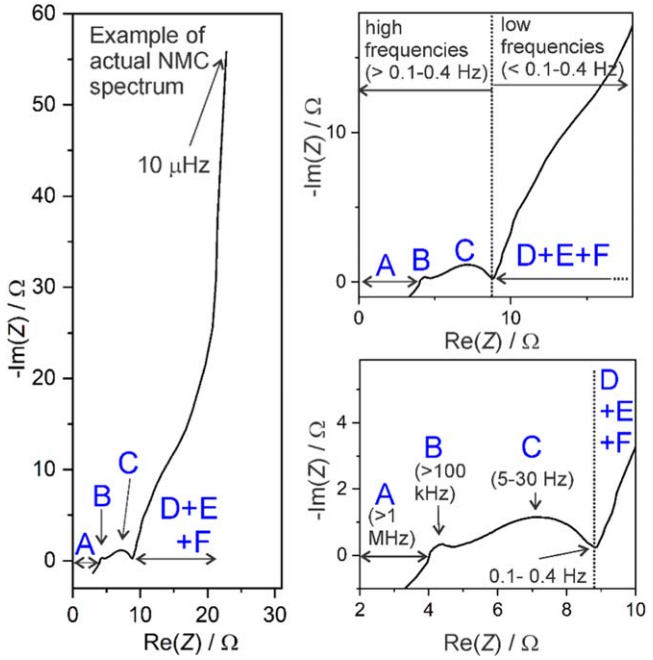

Figure 3. Realistic impedance spectrum obtained by measuring a symmetric NMC-NMC cell. Three different magnifications are shown in order to better recognize all the features. The correlation with the theoretical spectrum in Fig. 1c is indictated by the letters A-F. Typical frequencies are indicated. The arbitrary boundary between high- and low-frequency features is indicated by a dotted vertical line.

The mentioned deviations of the measurements from the ideal theoretical spectrum can have considerable effects on the result of the fitting, as shown in Fig. 4. Figure 4a shows the results of the sensitivity analysis in which the chemical capacitor describing the diffusion in the bulk electrolyte C_{14} is multiplied by a factor of 2 and 0.5 with respect to the base value of 8 F. These relatively large variations change the spectrum in the low frequencies (where the hump occurs) by only a fraction of an ohm (less than 3% of the hump size). Such a small change is comparable or even smaller than the experimental error, which means that the determination of C_{14} by fitting a similar measured spectrum would be very inaccurate.

In contrast, the same hump is very sensitive to the value of the exponent in the so-called constant phase element (CPE) which is often used in fitting procedures instead of pure capacitance. Before explaining this effect, let us first recall that the original physics-based model shown in Fig. 1b and discussed in previous papers,[1,2] does not include CPE elements. Mathematically, however, it is straightforward to introduce CPEs by replacing the impedance of the purely capacitive elements with the impedance of the correponding CPE element. In the case of impedance due to C_{04} ($Z(C_{04}) = 1/j\omega C_{04}$) the corresponding CPE is $Z(CPE) = 1/Q_{04}(j\omega)^{\alpha_{04}}$ where $j = \sqrt{-1}$ and ω is the angular frequency of the excitation signal.

In Fig. 4b, we change the value of α_{04} from 0.95 (a typical value used in this study, as we will show later) to 1 and then to 0.9. Even with such a relatively small variation of α_{04}, quite a large variation of impedance is observed in the region of the hump. The problem is that the physical meaning of the CPE elements is much less clear than that of the corresponding capacitances. In particular, unlike other parameters (Fig. 1), it is difficult to predict the behavior of the CPE exponents (α_i) when varying the mass loading. Furthermore, the sensitivity analysis has shown that in many cases of potential interest, the variation of certain physical parameters can be masked by the variation of a CPE exponent.

The simulations in Fig. 4c show the general effects of the inductive properties on the shape and magnitude of the impedance curves at the highest frequencies. In our particular case, the origin of

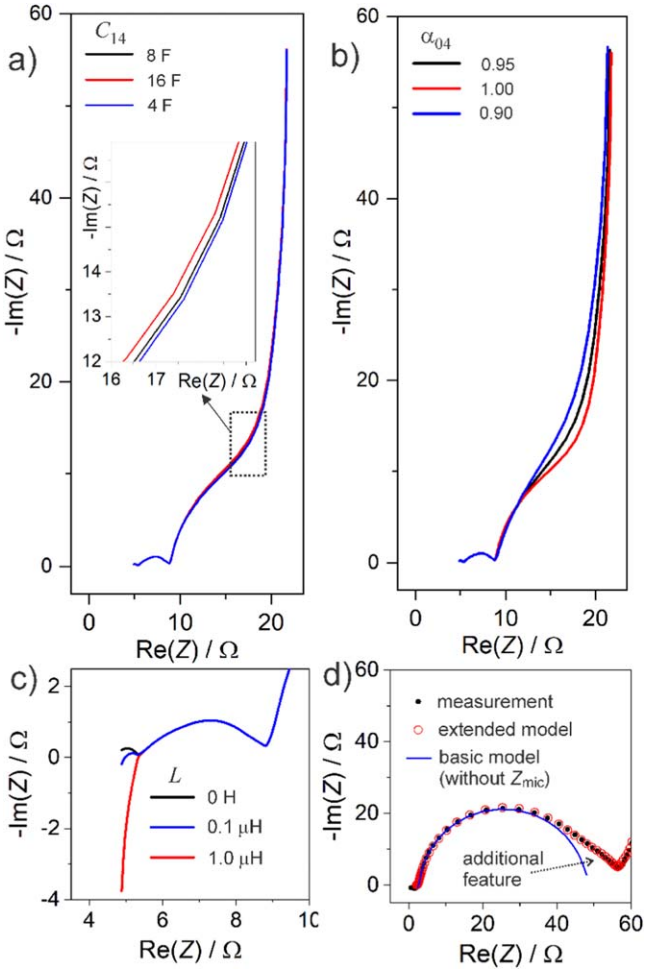

Figure 4. Effects of selected parameters on the shape and magnitude of the simulated impedance spectra. Black curves correspond to selected actual measurement whereas the red and blue curves show typical possible variations. (a) Effect of the variation in the magnitude of the chemical capacitance due to diffusion in the electrolyte-containing separator. (b) Effect of the exponent of the constant phase element associated with the chemical capacitance of the electrolyte in the pores of the separator (α_{04}), (c) Effect of the high frequency inductance (usually due to cables) in series with the model in Figs. 1b. (d) Identification of an additional feature that is not described in the model in Fig. 1b, but only briefly indicated as an additional element Z_{mic}.

the inductance was mainly due to the coaxial cables, which was confirmed by changing their length. To account for the inductive effect of the cables, an inductance in series was added to the model in Fig. 1b, the value of which varied within the expected values of the inductance of the cables (10^{-7} to 10^{-6} H for the present test setups). It can be clearly seen that the presence of inductance masks part of the predicted high-frequency range. This directly means that inadequate determination of the inductance for the given setup leads to errors in the determination of at least two features, i.e. the general features A and B shown in Figs. 1c and 3.

In the preliminary analysis of the measured spectra for different mass loadings, we also found discrepancies between the measured feature C and the predicted shape in Fig. 1c. An example of this discrepancy can be seen in Fig. 4d, where the blue line was obtained by fitting the model to the measured points (black dots). We have assumed that the right side of the measured arc contains an additional process, as shown in Fig. 4d. At present, it is unclear which additional process (to those contained in the model in Fig. 1b) occurs in the measured cells. Based on the relaxation time of this process (several seconds) and the microscopic examination of the

NMC material, it could be hypothesized that this additional feature represents diffusion in the liquid electrolyte present in the micropores of the NMC aggregates. If this is the case, the magnitude of this feature is expected to decrease approximately linearly with increasing electrode mass, which was indeed observed in the present measurements (see Figs. 6 and 7 in continuation). Despite this indication, we do not attempt here to extend the present physical model by accounting for the additional hypothesized diffusion processes in micropores, as such an extension would mean adding another dimension to the existing transmission line model and complicating the analysis considerably. Instead, we simply insert an arbitrary finite length transmissive Warburg element, Z_{mic}, (i.e. impedance due to micropore diffusion) at the positions indicated in Fig. 1b:

$$Z_{\mathrm{mic}} = R_{\mathrm{mic}} \frac{1}{\sqrt{i\omega\tau_{\mathrm{mic}}}} \tanh\sqrt{i\omega\tau_{\mathrm{mic}}} \qquad [5]$$

where R_{mic} is the resistance due to diffusion and $C_{\mathrm{mic}} = \tau_{\mathrm{mic}}/R_{\mathrm{mic}}$ is the corresponding chemical capacitance for this diffusion.

This transmissive nature of Z_{mic} is due to the fact that Li ions diffusing in the electrolyte in micropores eventually penetrate into the active particles, making this interface transmissive (permeable) for Li ions. The insertion of such an arbitrary diffusion element roughly describes the additional process seen in measured spectra (see the fit to the extended model in Fig. 4d) and thus compensates, at least mathematically, for the lack of a clear physical model at this point.

Finally, we would also like to address the question of the appropriate description of diffusion processes inside solid NMC particles. Let us first emphasize again that the NMC particles at hand are aggregates of smaller (primary) particles and individual aggregates in corresponding (pressed) cathodes show the whole range of observed mechanical damage—from some apparently intact to some partially cracked to highly disintegrated ones, where a large part of an aggregate has disintegrated into smaller chunks and sometimes even into primary particles (see FIB-SEM cross-section in PART-1). In addition, Mercury intrusion porosimetry (MIP) showed an increase in pore volume for all pressed cathodes with pores smaller than 100 nm. These pores are partly due to the compression of larger pores and partly to the formation of additional smaller pores due to the break-up of NMC aggregates.[15,16] In addition, the MIP analysis showed that there is a certain population of pores in the sub-20 nm range where no clear effect of pressing is observed (see PART-1). One possibility is that these micropores are due to the open porosity within the NMC aggregates. Accordingly, it can be expected that the NMC aggregates in the investigated cathodes exhibit considerable microporosity. The described contributions make it very difficult to determine the actual topology of the NMC interface between electrolyte and solid and thus the topology of the diffusion processes in solids.

Even if the presence of micropores is neglected, the significant distribution of aggregate size and the lack of clear knowledge about the nature of solid-state diffusion (spherical, linear, mixed, etc.) make an appropriate quantitative analysis of the corresponding impedance very difficult. To illustrate this, we show in Fig. 5a the effects of particle size distribution on the low-frequency solid-state diffusion impedance. The green curve shows the impedance spectrum due to solid-state diffusion in spheres of the same size. The red curve shows a simulation in which the particle size of the spheres varies in the same way as it was actually determined in the analysis of the particle size distribution of the present NMC aggregates in the SEM image (we selected 19 different sizes corresponding to the 19 main columns and weighted according to their numerical contribution to the total population of particles, see Fig. 1 in PART-1 of this study). The obtained simulated graphs were normalized to show the same total resistance of solid diffusion. More information about the simulation of the effect of particle size distribution on the impedance at low frequencies can be found in Supporting information S2.

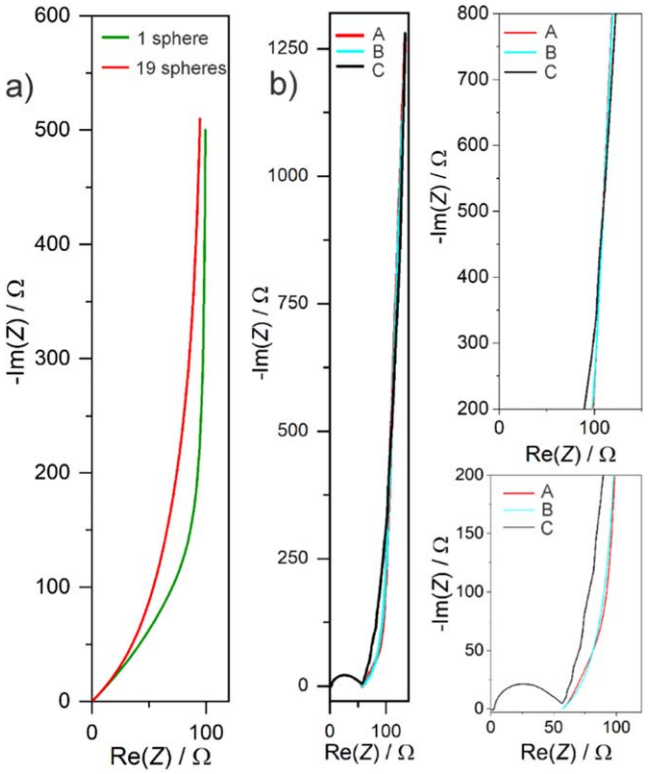

Figure 5. Low-frequency impedance response due to solid-state diffusion in active NMC particles. (a) The simulation shows the difference between the case where all particles have the same size (green curve) and the case where there are 19 different particle sizes (red curve). In both cases, spherical diffusion into the active particles was assumed. (b) Two selected simulations (A,B) normalized so that the low-frequency part matches the actual experimental data (C) as closely as possible (note that in this case the high-frequency impedance was not yet simulated). The simulated curve A assumes the same particle size distribution as in panel (a) (19 spheres, weighted by the microscopy data) + the contribution of the coupled diffusion of Li ions and anions in the separator. For comparison: In the simulated curve B, the diffusion in the separator is not taken into account. Both simulated curves show a similar deviation from the measured curve C.

Significant differences can be seen within the entire frequency range. In particular, the curve corresponding to the 19 distributed particle sizes shows a significantly greater slope over the entire frequency range shown (2 kHz to 0.2 mHz). Each change in the particle size distribution leads to slightly different characteristics of the impedance curve (not shown, but checked in the sensitivity analysis).

It can therefore be assumed that the addition of electrolyte-filled micropores, presence of aggregates etc. will further influence the shape of the curve. In contrast, the addition of known contributions (e.g. diffusion in the separator) has only a very minor effect on the model curve (e.g. Fig. 4a), i.e. this contribution is masked by the diffusion impedance in the solid state, so it would be difficult to assess it based on the analysis of measurements. Overall, we believe that with the current state of knowledge, it is extremely difficult to create a physically based simulation that accurately and unambiguously reproduces the actual impedance measurement corresponding to diffusion in solid microporous NMC aggregates. Such a simulation would require a precise morphological analysis of all parts of the electrode where diffusion can occur, as well as the determination of the statistical distribution of all these parts - which is well beyond the scope of this article.

To partially summarize this subsection, we can conclude that there are many factors that prevent the use of standard fitting methods as the main tool to identify impedance parameters at different mass loadings. This conclusion is further supported by the

analysis of the possible outcomes of the fitting the experimental curves with the present TLM in chapter S4 of the Supporting Information). Instead, we propose a combined approach, which is described in the next subsection.

A combined approach to determination of the scaling properties of model parameters.—Based on a detailed preliminary investigation of the measured impedance spectra at different mass loadings and a comprehensive sensitivity and fitting analysis of the proposed model (as partly demonstrated in Chapters S3 and S4 of the Supporting Information), we identified the conditions under which the extraction of each model parameter was most reliable. For example, feature C (interfacial arc at surface of NMC, see Fig. 1c) showed the largest and most pronounced impedances at the lowest loadings (2.3 and 5.2 mg). At the same time, the lowest loadings were also associated with a very low (almost negligible) contribution of parameters R_{03} and R_{05}. This means that at these low loadings, feature C was dominated by the charge transfer resistance R_{CT} and the double layer capacitance C_{DL}, so that their values could be determined quite reliably. The same applies to the parameters of the diffusion arc due to diffusion in micropores (R_w and C_w), which could be determined most reliably at the lowest loadings.

At least theoretically, determining the properties of bulk electrolytes is rather straightforward. These are determined by three elements: R_{13}, R_{15} and C_{14}, which are responsible for two theoretical characteristics: the high frequency section A (the so-called electrolyte resistance) and the diffusion arc E (see Fig. 1c). Let us neglect the feature E for a moment, because in real spectra the arc E is hidden in the low-frequency, closely coupled section, which is labeled D+E+F in Fig. 3. On the other hand, the electrolyte resistance (high-frequency section A) is usually clearly defined, even if the data can be affected by cable inductance and other interference effects, as described in Problems occurring in fitting the present spectra section. Nevertheless, a more or less reliable average value for high-frequency section A can be determined by carrying out many measurements. If this approach does not work well, it is possible to measure the electrolyte properties in separate cells without other components, i.e. without a cathode in our case. Finally, we also point out that electrolyte conductivities are usually reported in a number of studies and these values can also be used as reference values for evaluating the given electrolyte resistance contributions (taking into account separator geometry, porosity and tortuosity). In the present study, we relied on our separate measurements of the electrolyte in cathode-free cells, which gave us well-estimated contributions to all three parameters, R_{13}, R_{15} and C_{14}.

Similar to the contribution of the bulk electrolyte, the impedance of the electric contact between the current collector and the electrode assembly is frequently clearly observed as a well-separated arc B at high frequencies. In most current studies, the properties of the aluminum substrate are well optimized (e.g. carbon-coated) so that arc B is relatively small compared to the other contributions. On the contrary in the past when using "bare" (non-coated) aluminum foil contribution of contact arc B was much larger—typically ranging from a few to few tens of Ω cm^2, depending upon electrode preparation procedure and force applied to a cell.[6,7] In this study, arc B was sometimes well resolved, while in other cases it was masked with inductive and other high-frequency contributions. We calculated the average values of R_A and the sum $C_B + C_C$ from the better-resolved measurements and then assumed that the same average values would apply to the poor-resolution arc B measurements.

Next we describe the determination of the model parameters that describe the transport through the electrolyte in the pores of the porous electrode, R_{03}, R_{05} and C_{04}. These parameters influence the size and shape of features C and D in Fig. 1c. As already mentioned, feature C is also influenced by the values of R_{CT} and C_{DL}. However, the nature of the scaling of the first three elements is exactly opposite to the last two (see Fig. 2). More precisely, R_{03}, R_{05} and C_{04} increase with electrode thickness, while R_{CT} and C_{DL} decrease. We took advantage of this property and fitted the features C and D at the highest mass loading by assuming a negligible contribution of R_{CT} and C_{DL}.

The last parameters that had to be determined are those that describe the solid state transport within the NMC aggregates. Originally this was described by the finite-length Warburg diffusion, Z_W, see Fig. 1b. However, as explained in the previous chapter, it is very difficult to construct a reliable, very detailed physical model that would fit well to the measured impedance of this solid-state diffusion. Therefore, we decided to describe this part of the impedance purely mathematically with a set of 5 R-CPE elements without attempting to assign any physical meaning to the individual elements in this set. However, this did not affect the primary objective of this study, which was to determine the quality of the scaling of the different contributions in the transmission line model. In particular, we expected that describing diffusional impedance with a series of R-CPE elements would give us the same information about the scaling properties of the solid-state diffusion process as if we used the original physical element, namely the inverse proportionality to mass loading, as shown in Fig. 2. Specifically, the numerical expression for Z_w was obtained by fitting the low-frequency part of the lowest mass loading (2.3 mg per 2 cm^2). Indeed, it was reasonable to assume that at the lowest loading, the low-frequency impedance section consisted only of features E+F, while feature D was negligible (as explained above). Since we knew the contribution of the electrolyte (E), we fixed the corresponding resistors and capacitor and added 5 R-CPE elements that determine the unknown Z_w, as explained above. By fitting, we obtained a good approximation for Z_w at the lowest mass loading and could readily calculate its value for all other loadings (assuming the theoretically expected relationship $Z_w \propto$ 1/electrode mass, see Fig. 2). In order to distinguish the mathematically (numerically) determined solid-state diffusion impedance from its physical counterpart (Z_w), we generally refer to the former as Z_{diff} and for the special case of 2.3 mg electrode this impedance is referred to as $Z_{diff,0}$.

To summarize this part, we have carefully chosen the optimal way to determine the value of each of the 13 model parameters, either from given experiments, from sets of the most reliable experiments, or from other sources (as in the case of the electrolyte parameters). These 13 fixed parameters are highlighted in bold in Table II. The parameters for all other loads were considered unknown and calculated based on the respective scaling laws, which are explained in detail in Fig. 2. In total, this means that we calculated 91 unknown parameters on the basis of which we were able to create Table II. The data in this table was then used to construct the theoretical impedance spectra for all measured loads, as described in the next chapter.

Table II. The values of all model parameters as determined using the combined approach proposed in this paper. The values of the parameters of the 5 R-CPE elements that describe Z_{diff} ($Z_{diff,0}$) at lowest mass loading, $m_0 = 2.3$ mg, are the following: $R_1 = 2.311$, $Q_1 = 1.457$, $\alpha_1 = 0.94269$, $R_2 = 209.3$, $Q_2 = 1.457$, $\alpha_2 = 0.91462$, $R_3 = 22.32$, $Q_3 = 1.025$, $\alpha_3 = 0.75585$, $R_4 = 9174$, $Q_4 = 7.074$, $\alpha_4 = 1.217$, $R_5 = 160.3$, $Q_5 = 32.93$, $\alpha_5 = 1.214$ where R_i, Q_i and α_i correspond to:

$$Z_{diff,0} = \sum_i Z_i = \sum_i R_i/(1 + R_i Q_i (j\omega)^{\alpha_i}) \qquad [6]$$

with all resistances R_i in units Ω and parameters Q_i in units $s^{\alpha_i}\Omega^{-1}$.

Results of theoretical analysis using the combined approach introduced in this paper.—Figures 6 and 7 compare the experimental data for different loadings with impedance simulations using the data in Table II. We note once again that 7 out of 8 simulated graphs are predictions based on a set of fixed model parameters for a selected loading, as described above. Considering this fact, we estimate that the simulated graphs agree quite well with the measurements. This assertion may seem rather bold at first glance,

Table II. Parameters of the impedance model for all electrodes examined in the present study. Only the parameter values in bold were determined independently (in different ways, as explained in the notes below the table and in the main text), all other 91 parameters were calculated from scaling laws. The values in this table were used to create all the curves in Figs. 6 and 7. Note that C_{DL} was replaced by a constant phase element with an exponent of 0.95 in the simulations. This reflects the realistic response of the electrode due to the pores within or between the carbon and binder domain clusters (as determined by Hg porosimetry, see PART-1). Similarly, Warburg diffusion in the micropores of the NMC aggregates was modeled using an anomalous diffusion model with an exponent value of 0.88. The value of electronic resistance, R_{01}, was assumed to be 0 in all cases.

m [mg]	R_A [Ω]	C_B, C_C [μF]	R_{CT} [Ω]	C_{DL} [mF]	R_{13} [Ω]	C_{14} [F]	R_{15} [Ω]	R_{03} [Ω]	C_{04} [F]	R_{05} [Ω]	Z_{diff} [Ω]	R_{mic} [Ω]	C_{mic} [F]
2.3	0.25	**1**	**20.0**	**1.10**	**8**[a)]	**10**[b)]	**2.96**[a)]	0.86	2.24	0.32	$\mathbf{Z_{diff,0}}$[c)]	**7.5**	**0.066**
5.0	0.25	1	9.54	2.31	8	10	2.96	1.14	2.42	0.42	$\frac{m_0}{m} Z_{diff,0}$	3.579	0.14
11.1	0.25	1	4.51	4.88	8	10	2.96	1.54	2.36	0.57	$\frac{m_0}{m} Z_{diff,0}$	1.690	0.29
22.5	0.25	1	2.21	9.94	8	10	2.96	3.14	4.80	1.16	$\frac{m_0}{m} Z_{diff,0}$	0.830	0.59
29.9	0.25	1	1.68	13.1	8	10	2.96	4.00	5.83	1.48	$\frac{m_0}{m} Z_{diff,0}$	0.630	0.79
39.6	0.25	1	1.26	17.4	8	10	2.96	5.14	7.17	1.90	$\frac{m_0}{m} Z_{diff,0}$	0.474	1.04
49.3	0.25	1	1.02	21.6	8	10	2.96	6.28	8.55	2.33	$\frac{m_0}{m} Z_{diff,0}$	0.381	1.30
58.5	**0.25**	1	0.86	25.7	8	10	2.96	**8.00**	**12.00**	**2.96**	$\frac{m_0}{m} Z_{diff,0}$	0.321	1.54

a) Determined from separate impedance measurements of electrolyte. b) Estimated from the volume and concentration of electrolyte in separator. c) Determined from fitting using 5 R-CPE elements in series.

as there are obvious discrepancies between the measurements and the predicted spectra (for example, there are clear deviations at high frequencies in Figs. 6c or 7g). However, a more comprehensive analysis shows a good prediction of almost all trends and in some cases even a quantitative prediction of the measured impedance quantities.

For example, we can see that feature C (as defined in Fig. 1c) resembles a semicircle at low loadings, but then transforms into a much more suppressed shape at higher loadings. This well-known phenomenon is due to a significant decrease in RCT and a simultaneous increase in R_{03} and R_{05} (the parallel coupling of R_{03} and R_{05} forms the ionic resistance in the electrode, Rion) with increasing mass loading.[17] Simultaneously with this change in shape, the magnitude of feature C decreases from about 50 to only 3 Ω at the thickest loading, and the simulation follows the measured trend quite well. It is true that for certain intermediate masses (e.g. 11 mg, 29 mg, 49 mg) the size of this central arc deviates considerably from the measurements. However, these deviations are obviously scattered, with some predictions giving an arc that is too large and others too small. In our opinion, these scattered predictions are a sign that the model is sound and that the errors are mainly due to difficulties in the preparation of the electrodes and/or the measurements.

The dynamics of the simulated spectra with increasing loading also follow well those of the measured spectra at low frequencies. At the lowest loading, this part consists more or less of a slightly inclined vertical line (the so-called low-frequency "impedance tail"), with the imaginary part exceeding 1 kΩ at the lowest frequency (10^{-4} Hz). As the loading is increased, a "hump" appears in the lower part of this vertical line, which becomes more and more pronounced—both in the measured and simulated spectra. The appearance of this "hump" is due to the decrease in Z_{diff}, so that electrolyte ionic contributions R_{03}, R_{05}, R_{13} and R_{15} become more prominent, i.e. contribute to the size of the electrolyte transport arc. Finally, the solid diffusion impedance, Z_{diff}, seems to scale best of all features—in agreement with the empirical observations in PART-1 of this study. In particular, a comparison of the measured and simulated (theoretically predicted) impedance values at the lowest frequency (10^{-4} Hz) shows agreement within a few percent for all loadings studied (see Figs. 6 and 7). At this rather low frequency, the impedance is mainly determined by the chemical capacitance of the active material. This confirms the earlier empirical findings,[9,18,19] that low-frequency impedance spectroscopy is an accurate method for detecting the amount of active mass in a given electrode.

The worst part of the prediction probably relates to the highest frequencies, where the so-called contact resistance dominates—together with the electrolytic resistance, both of which are influenced by the inductance of the cables. It is well known that the contacts and cables are difficult to control experimentally. In addition, their impedances are small, so any deviation quickly leads to large relative errors.

The good agreement between the measured and predicted trends justifies the creation of graphs showing some general scaling trends of all relevant model parameters used in this study. To do this, we simply use the values of the parameters calculated in Table II. In this context, it is helpful to recall the definition of total electrode resistance for electrodes that exhibit good electronic conductivity, which is defined by Eq. 3. Here we recall that for spherical geometry the parameter ξ acquires a value of 5 which is probably the most appropriate for use in this study (see Fig. 5 and chapter S2 in Supporting information). However, it has to be further noted that instead of R_w we use here a mathematical construction that replaces this physical parameter and is denoted as Z_{diff}, as explained above.

Finally, we point out again that we had to introduce an additional parameter in this work, which is due to the diffusion of ions in the micropores of the active NMC aggregates. We refer to the resistive part due to this additional impedance-resistance parameter simply s R_{mic}. This is then added to the total resistance of the electrode (i.e. to Eq. 3) as $R_{mic}/3$.

Figure 8 shows all contributions to the total resistance of the electrodes as a function of the mass loading. It is quite clear that different parameters make the greatest contribution at different loadings. As expected, Z_{diff} and R_{CT} predominate at low loadings, while R_{13} and R_{03} (Li^+ ion resistance of the electrolyte phase in the pores of the separator and the NMC cathode) begin to dominate at the highest loadings. The contact resistance (R_A) makes the smallest contribution at all mass loadings (due to the good electrical contact with the carbon-coated aluminum current collector). Except for very small or very high loadings (e.g., such as in the industrial manufacture of electrodes), it is not appropriate to neglect any contribution, as they all have a significant effect on the overall resistance of the electrode.

It is very important to point out that a simple analysis of the EIS spectra neglecting the transport limitation of ions in the separator and within the porous electrode in the case of thick (industrially realistic) electrodes (corresponding to an NMC loading of about 30 mg in the present study or about 15 mg per 1 cm^2 of the geometric surface of the aluminum substrate) would lead to incorrect

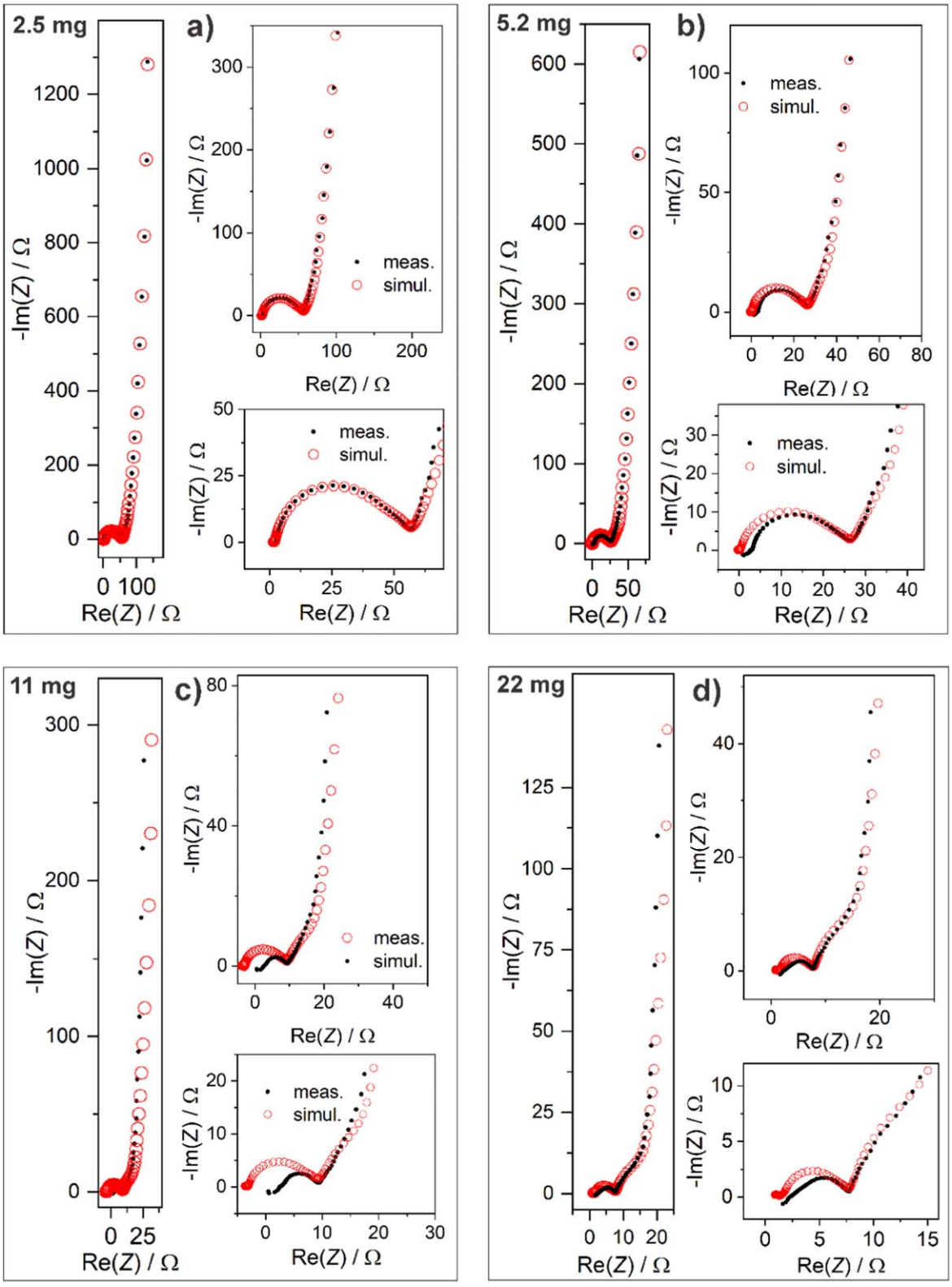

Figure 6. Measured (filled black circles) and simulated (red open circles) impedance responses of NMC electrodes with masses ranging from 2.3 mg to 22 mg. In all cases, the geometric surface area was 2 cm^2. The simulations were carried out according to the combined approach introduced in this paper. Each spectrum is shown in three magnifications in order to better recognize the agreement and deviations between the measurements and the simulations in different frequency ranges. For a balanced view of the deviations at high and low frequencies, we positioned the simulated spectra so that the impedance values of the measured and model spectra match at the point of transition from the high-frequency arc to the low-frequency vertical curve (diffusion impedance). Due to this "artificial shift," some modeled spectra can extend to negative values on the real axis.

results and interpretations. For example, attributing the real part (Re (*Z*)) of the low-frequency impedance solely to the solid-state diffusion process of the Li component within the NMC particles, without taking into account the transport limitations of the ions in the porous electrode, would lead to a significantly underestimated value of the chemical diffusion coefficient of lithium. This error

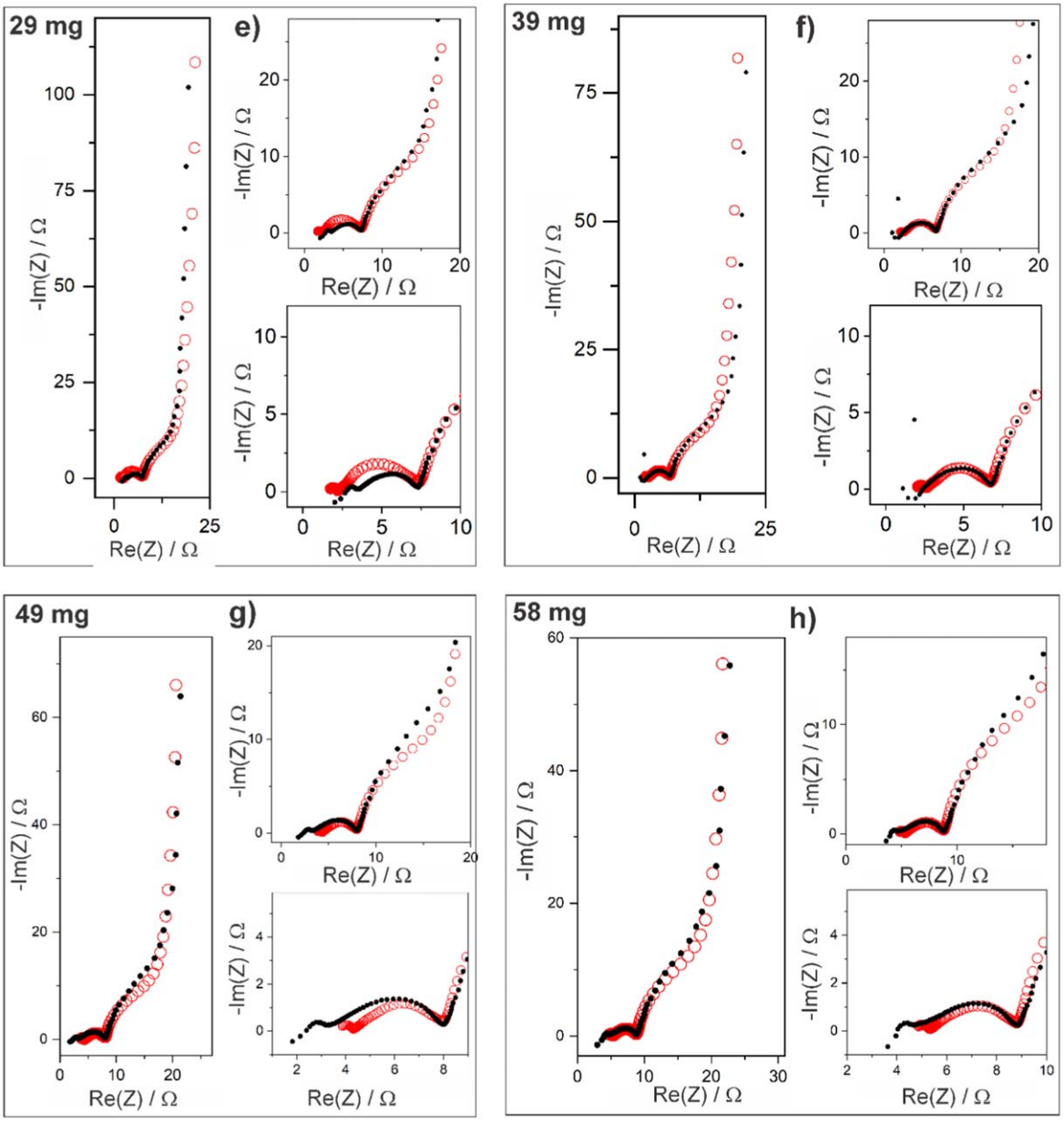

Figure 7. Measured (filled black circles) and simulated (red open circles) impedance responses of NMC electrodes with masses ranging from 29 mg to 58 mg. In all cases, the geometric surface area was 2 cm^2. The simulations were carried out according to the combined approach introduced in this paper. Each spectrum is shown in three magnifications in order to better recognize the agreement and deviations between the measurements and the simulations in different frequency ranges. For a balanced view of the deviations at high and low frequencies, we positioned the simulated spectra so that the impedance values of the measured and model spectra match at the point of transition from the high-frequency arc to the low-frequency vertical curve (diffusion impedance). Due to this "artificial shift," some modeled spectra can extend to negative values on the real axis.

would be even more drastic for high-energy NMC electrodes with a much lower porosity (typically in the order of 20%) and additionally due to the associated higher tortuosity. This study thus clearly shows the necessity of using appropriate analysis tools (such as the present TLM) to interpret the measured impedance in the entire frequency range, including the lowest frequencies.

Conclusions

A detailed analysis of the measured impedance spectra of NMC cathodes with significantly different masses (thicknesses) has shown that all theoretically expected contributions (labeled from A to F in Fig. 1c) actually occur in the measurements of realistic cathodes. We have also confirmed the theoretically expected scaling relationships developed and discussed for all model parameters in the first part of this article. Probably the most important practical implication of these scaling properties is that for a given electrode mass, only some impedance contributions (labeled A-F in Fig. 1) are detected, while the others are too small to be detected (i.e., they are within the measurement error). Thus, if we really want to determine all (or most) model parameters from impedance measurements, the measurements of electrodes with (very) different masses seems almost unavoidable. An alternative option could be to make a set of electrodes with a wide range of well-defined porosity and tortuosity, but probably varying the mass loading is the easiest way to make well-controlled measurements.

From the trends shown in Fig. 8, we can estimate that a minimum of total resistance is reached at about 25-30 mg per 1 cm^2, which in

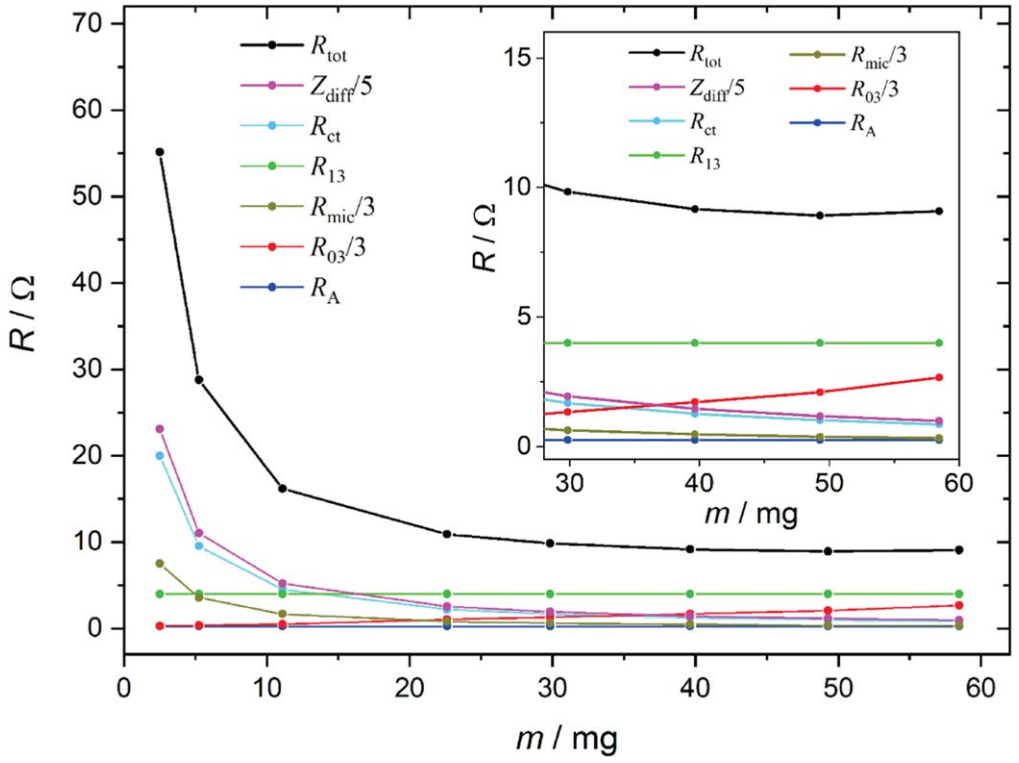

Figure 8. All contributions to the total resistance of the electrode (R_{tot}, see Eq. 3) for all mass loadings investigated in this work. The inset shows an increase at high loadings.

the case of the present NMC electrodes (with typical porosities of about 40%–45%) can be considered as the optimum thickness causing minimum ohmic losses—in the case of a linear excitation signal (e.g. small C-rates).

Finally, the present analysis revealed an unexpected contribution to the measured impedance spectra (not predicted in Fig. 1c). This contribution showed an inverse proportionality to mass, i.e. it was mainly observed for (very) thin electrodes. We attributed it to the diffusion of charged mobile ions (lithium ions, anions) in the micropores of the aggregates seen in the present active material. At present, this is still a hypothesis that needs to be confirmed in future work.

Acknowledgments

Jože Moškon thanks the Slovenian Research Agency for financial support in the framework of project J2–4463. Robert Dominko thanks the Slovenian Research Agency for financial support in the framework of national program no. P2–0423. Miran Gaberšček thanks the Slovenian Research Agency for financial support in the framework of national program no. P2–0393.

ORCID

Jože Moškon https://orcid.org/0000-0002-8223-0031
Miran Gaberšček https://orcid.org/0000-0002-8104-1693

References

1. J. Moškon, J. Žuntar, S. Drvarič Talian, R. Dominko, and M. Gaberšček, *J. Electrochem. Soc.*, **167**, 140539 (2020).
2. J. Moškon and M. Gaberšček, *J. Power Sources Adv.*, **7**, 100047 (2021).
3. L. Froboese, P. Titscher, B. Westphal, W. Haselrieder, and A. Kwade, *Mater. Charact.*, **133**, 102 (2017).
4. S. Drvarič Talian, J. Moškon, R. Dominko, and M. Gaberšček, *ACS Appl. Mater. Interfaces*, **9**, 29760 (2017).
5. K. Zelič, T. Katrašnik, and M. Gaberšček, *J. Electrochem. Soc.*, **168**, 070543 (2021).
6. M. Gaberscek, J. Moskon, B. Erjavec, R. Dominko, and J. Jamnik, *Electrochem. Solid-State Lett.*, **11**, A170 (2008).
7. J-M. Atebamba, J. Moskon, S. Pejovnik, and M. Gaberscek, *J. Electrochem. Soc.*, **157**, A1218 (2010).
8. M. GABERSCEK and J. JAMNIK, *Solid State Ionics*, **177**, 2647 (2006).
9. M. Gaberscek, M. Küzma, and J. Jamnik, *Phys. Chem. Chem. Phys.*, **9**, 1815 (2007).
10. J. Jamnik, *Solid State Ionics*, **157**, 19 (2003).
11. C. Ho, I. D. Raistrick, and R. A. Huggins, *J. Electrochem. Soc.*, **127**, 343 (1980).
12. T. Jacobsen and K. West, *Electrochim. Acta*, **40**, 255 (1995).
13. M. GABERSCEK, R. DOMINKO, and J. JAMNIK, *Electrochem. Commun.*, **9**, 2778 (2007).
14. M. Gaberscek, *J. Power Sources*, **189**, 22 (2009).
15. T. Beuse, M. Fingerle, C. Wagner, M. Winter, and M. Börner, *Batteries*, **7**, 70 (2021).
16. C. Schilcher, C. Meyer, and A. Kwade, *Energy Technol.*, **4**, 1604 (2016).
17. R. Morasch, J. Keilhofer, H. A. Gasteiger, and B. Suthar, *J. Electrochem. Soc.*, **168**, 080519 (2021).
18. M. D. Levi and D. Aurbach, *J. Phys. Chem. B*, **101**, 4630 (1997).
19. D. Aurbach, M. D. Levi, O. Lev, J. Gun, and L. Rabinovich, *J. Appl. Electrochem.*, **28**, 1051 (1998).